THE JOURNAL OF PHYSICAL CHEMISTRY C

Article

pubs.acs.org/JPCC

Phonon Anharmonicity of PdO Studied by Raman Spectrometry

Zhouying Zhao, Jacqueline Elwood, and Michael A. Carpenter*

Colleges of Nanoscale Science and Engineering, SUNY Polytechnic Institute, Albany, New York 12203, United States

ABSTRACT: Raman spectra were measured for palladium oxide (PdO) at temperatures from 298 to 973 K. The first-order scattering B_{1g} and E_g phonon modes show prominent frequency and line width dependencies on temperature. The phonon behaviors are described well by a model considering contributions from thermal expansion related quasiharmonicity and explicit lattice anharmonicity from both cubic and quartic phonon decay processes. Compared to the quasiharmonicity for the line shift, the explicit anharmonicity is found to be relatively smaller for the B_{1g} mode with the cubic anharmonicity leading the quartic term. The E_g mode has a smaller line shift which mostly follows a quartic phonon decay mechanism while the cubic contribution is canceled by thermal expansion effects. The cubic anharmonicity dominates mostly the line broadening with more prominent quartic effects responsible for the larger broadening of the E_g mode. Multiple potential asymmetric cubic and quartic anharmonic decay channels including down-conversion and up-conversion are identified with their characteristics discussed and correlated to the positive and negative anhamonicities found for the two phonon modes studied.

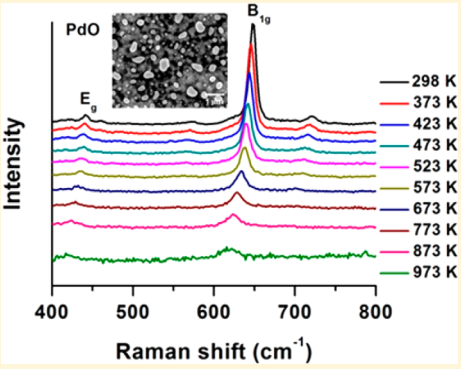

INTRODUCTION

PdO is a catalytically active material and has found extensive use in heterogeneous and homogeneous catalysis for chemical conversions, energy production, and pollution mitigation based on the reversible and energetic creation of Pd^{2+} or oxygen vacancies in the oxide.[1−6] The material is also an appreciable source of oxygen because of its reversible equilibrium transformation with Pd at elevated temperatures within a sealed cavity. This characteristic has been employed as an oxygen reference material in the development of harsh environment oxygen sensors.[7] Owing to the technological interest in the oxide as a critical component in a variety of applications, the material has been actively studied. Crystalline PdO has a tetragonal cooperite structure (space group D_{4h}^9-$P4_2/mmc$) and is composed of edge-sharing chains of PdO_4 planes.[8,9] Strong resonance Raman scattering has been observed from PdO at room temperature, with the resonance enhancement possibly correlated to an exciton model of the electronic structure.[10]

The temperature dependence of Raman scattering carries a great deal of information on the interactions of the vibrational phonon modes at the Brillouin zone center. The phonon line shift and broadening with temperature can be understood through a determination of the lattice anharmonicity properties. It has been shown in the literature that for a variety of materials studied the temperature-dependent phonon properties can be modeled by the effects of thermal expansion, phonon−phonon coupling, and perhaps electron−phonon coupling, depending on the specific material and electronic structures.[11−16] Anharmonic effects in crystals strongly affect a number of processes including energy transport,[17,18] structural phase transformation,[19] optical properties,[20] and electronic transport in devices,[21,22] which contributes to the functionality of the material. Surprisingly, no data and knowledge exist so far on the phonon scattering temperature dependence and the lattice anharmonicity character for PdO. Studying the phonon properties at the atomistic level is essential to both a fundamental understanding and functional improvement of the material, such as for improving the catalysis efficiency at elevated temperatures[1] that involves phonon driven thermal processes as a key step. Furthermore, many questions remain about the complex properties related to the detailed surface redox processes, definite electronic structure, oxygen vacancies, phonon dynamics, and size-dependent bulk and surface/interface effects.[23−26]

In this paper, we present experimental and theoretical analyses of the temperature-dependent behaviors of the zone-center phonons in PdO. Phonon scattering is characterized for stress-relaxed PdO crystals at temperatures from 298 to 973 K by *in situ* Raman spectroscopy under well-controlled conditions and analyzed by modeling of the measured temperature dependence. This work reveals a characteristic picture of nonlinear lattice dynamics in PdO, which illustrates how the cubic anharmonicity of three-phonon processes and the quartic anharmonicity of four-phonon processes distinctly influence the line shift and broadening of the B_{1g} and E_g Raman modes, in addition to the contribution of the volume-dependent quasiharmonicity. It also demonstrates that identifying the phonon decay channels based on the phonon dispersion information is important for understanding the detailed

Received: August 6, 2015
Revised: September 17, 2015
Published: September 17, 2015

DOI: 10.1021/acs.jpcc.5b07652
J. Phys. Chem. C 2015, 119, 23094−23102

phonon anharmonic behaviors. Furthermore, with this analysis the isobaric mode Gruneisen parameter, the anharmonic constants of cubic and quartic phonon coupling processes, and phonon line frequency and line width, extrapolated to 0 K, are obtained. The modeled data below 300 K serve as a baseline of information for this highly functional material.

MATERIALS AND METHODS

PdO crystal samples were prepared by oxidation of metallic Pd thin films followed by high temperature redox treatments for stress relaxation. The 90 nm Pd films were deposited on silicon, quartz, or yttria stabilized zirconia (YSZ) coated quartz substrates using rf sputtering and then annealed at 973 K in 15% O_2−85% N_2 gas ambient for 7 h for complete oxidation as confirmed by post-XPS analysis. To release the observed stress from the substrates, the as-prepared PdO samples were further annealed at 1073 K in Ar for 2 h for decomposition and growth of larger Pd particles. This was followed by a subsequent reoxidation at 923 K in the same oxygen containing gas environment as mentioned above for 19 h and cooled to room temperature at a slow rate of 1.2 K/min. A high temperature cell (15 mL internal volume) was used for micro-Raman scattering measurements at temperatures from 298 to 973 K in a stagnant gas environment. Prior to the measurement, the loaded sample was pretreated to 973 K in 400 sccm of 5% O_2 in Ar for 3 h for oxidative cleaning or preconditioning. The reason for the 973 K high temperature limit is that the PdO was found to partially decompose at temperatures above this value. A critical point for this study is an accurate measurement of the sample temperature. To do so, a thermocouple was mounted on the sample surface to ensure an accurate temperature reading at a spot near the Raman scattering interrogation location. In addition, following the preoxidative treatment, the gas flow was held stagnant to ensure there was no appreciable convective cooling of the sample. A Renishaw Raman 2000 system was used to acquire the Raman scattering spectra which had a spectral resolution of 1 cm^{-1}. The acquisition was run for a 10 s exposure time for collection of a single spectrum with a 514.5 nm laser excitation source after 30 min of stabilization at each temperature step. Before the measurement, the Raman tool was calibrated with a crystalline Si wafer with the characteristic peak observed at 519.6 cm^{-1}. A low laser power of 0.1 mW (power density of 8 $\mu w/\mu m^2$) on the sample was used in all tests to avoid laser heating without using any neutral density filters. The experimental spectra were analyzed with theoretical models that include phonon−phonon interactions and thermal expansion effects and possible phonon decay channels identified. These models were used for determining the phonon anharmonic behaviors within the PdO crystals and extrapolating the fundamental spectral parameters at 0 K. Environmental scanning electron microscopy (E-SEM) was used to examine the sample surface morphologies and particle sizes.

RESULTS AND DISCUSSION

High temperature oxidation of the 90 nm sputter deposited Pd films yields lustrous metallic-green crystals of PdO. The as-prepared PdO films are small-grained, continuous, and well bonded to the substrates, experiencing, however, some stress from the substrates according to the Raman spectral characterization. Raman peaks of the as-prepared PdO on quartz substrates were observed to be more downshifted relative to that with YSZ coated quartz or Si substrates. The frequency downshift with the substrates results from the differential thermal expansion of the substrates (at 293 K the volume thermal expansion coefficient is 19.5 × 10^{-6} K^{-1} for PdO, 1.77 × 10^{-6} K^{-1} for quartz, ∼10 × 10^{-6} K^{-1} for YSZ, and 9 × 10^{-6} K^{-1} for Si), leading to a tensile stress development in the PdO films after the oxidative annealing process. It has been noted in the literature that stress effects from substrates on measured Raman data of thin films are a difficult issue and may limit an accurate determination of the temperature dependence of the Raman modes or anharmonic phonon dynamics in materials.[14,16,27,28] Buffer layers or sophisticated fabrication of free-standing nanostructures have been previously used to minimize the stress/strain issues.[16] In this work, we introduced a simple method by high temperature redox treatment of the as-prepared samples for regrowth of relaxed and large-grained (e.g., 500 nm) PdO crystals, which renders minimized substrate effects. The resultant film morphology is shown by the representative SEM image of PdO on a Si substrate, which is compared to that before the treatment (Figure 1). The film

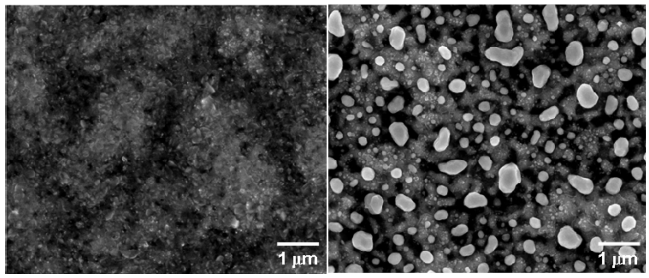

Figure 1. SEM images of PdO grown on Si substrate before (left) and after (right) high temperature redox treatments.

turned nonlustrous dark gray with formation of a rough morphology. Correspondingly, the Raman bands (identified below) from PdO deposited on three different substrates are observed to overlap very well with one another (Figure 2) and

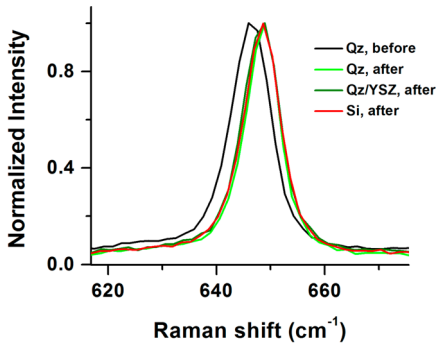

Figure 2. Comparison of Raman spectra of PdO grown on different substrates before and after high temperature redox treatment as labeled.

are upshifted relative to that from the untreated film on quartz substrates in the figure. Given the disparities in the substrate types and the annealing treatments, while it cannot be confirmed, one can surmise that these films are stress relaxed. The following Raman analysis is therefore focused on the PdO crystals on a Si substrate unless mentioned otherwise.

A typical full Raman spectrum from a PdO sample at room temperature is shown in Figure 3. The main sharp peak

DOI: 10.1021/acs.jpcc.5b07652
J. Phys. Chem. C 2015, 119, 23094−23102

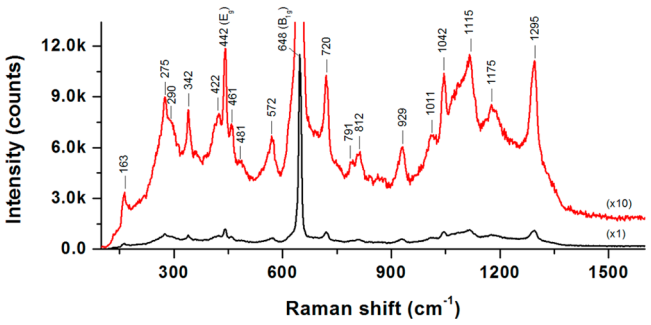

Figure 3. Full Raman spectra of a typical PdO sample at room temperature. The upper curve is a magnification of the lower curve for revealing the most prominent features as labeled.

centered at 648 cm^{-1} is the first-order scattering from the Raman-active B_{1g} phonon mode, which involves only O motion along the *c*-axis. Another first-order Raman scattering mode at 442 cm^{-1} is identified as the E_g mode and has O motion perpendicular to the *c*-axis. Figure 4 displays the vibrational

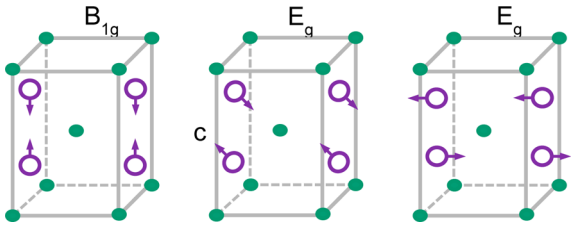

Figure 4. B_{1g} and E_g Raman-active phonon vibration modes in crystalline PdO. Pd atoms (small green solid circles) occupy D_{2h} sites, and O atoms (large violet open circles) occupy D_{2d} sites, in the crystal of tetragonal space group D_{4h}^9.

orientations of the B_{1g} and E_g Raman modes relative to the *a*- and *c*-axes in the lattice unit cell of the tetragonal PdO crystal. These two bands are accompanied by multiple smaller peaks displayed more clearly within the 10× magnified spectrum in the figure, which are attributed to second-order scattering processes from overtones and combinations or to forbidden LO-phonon scattering, according to the study by McBride et al.[10] The B_{1g} peak is symmetric and sharp, consistent with the formation of larger PdO particles in the samples and with bulk-like film properties. In fact, PdO is very Raman-active, and an oxide of less than 1 nm thickness is readily detectable by Raman scattering[29] without the need for an external enhancement approach using, for instance, plasmonic Au nanoparticles due to its resonant Raman scattering property.

The samples display strong temperature-dependent Raman scattering characteristics. As shown for a typical PdO sample on Si (Figure 5), the Raman bands progressively dampen, downshift, and broaden with temperatures increasing from 298 to 973 K, where the intensity axis is set in a logarithm scale for a clearer data presentation. The B_{1g} and E_g bands were fitted with a single Lorentzian function for extraction of the peak position and full width at half-maximum (fwhm), with the fitting results displayed as a function of temperature in Figure 6. Three sets of data collected for the sample on Si substrates are presented in the figure and were averaged as a function of temperature for the modeling analysis below. As shown, the B_{1g} mode undergoes a larger phonon softening but smaller line broadening with temperature relative to that of the E_g mode. The nonlinear temperature dependence of the phonon

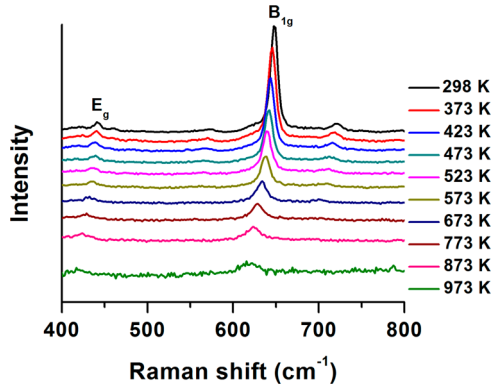

Figure 5. Raman spectra of PdO at different temperatures. The intensity axis is set in logarithmic scale for a clearer exhibition of the smaller bands at elevated temperatures.

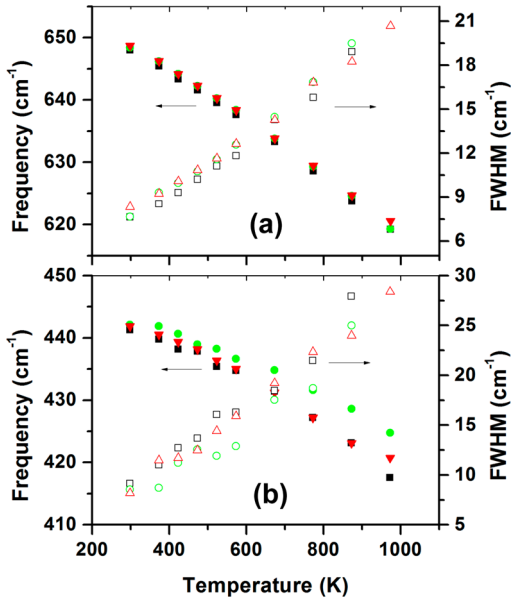

Figure 6. Three measurements of temperature-dependent Raman frequency and fwhm of the B_{1g} (a) and the E_g (b) modes of PdO.

frequency and line width (inverse of phonon lifetime) is an indication of nonharmonic lattice dynamics due to the phonon anharmonicity and volume thermal expansion effects. The inherent presence of anharmonic forces in a crystal lattice causes energy interchange between harmonic phonon normal modes, thus driving thermal equilibrium within the lattice.

Specifically, according to the lattice dynamic theory of anharmonic crystals, there is an anharmonic self-energy for optical phonon modes, with the real and imaginary parts of the complex term measuring a frequency shift and a dampened line width of the modes, respectively.[30−32] The temperature dependence of the phonon mode frequency $\omega_j(T)$ at constant pressure is expressed as

$$\omega_j(T) = \omega_{oj} + \Delta\omega_j(T)_V + \Delta\omega_j(T)_{anh} \quad (1)$$

where ω_{oj} is the harmonic frequency which is independent of temperature with *j* being the mode index, $\omega_{oj} + \Delta\omega_j(0)_{anh}$ is the anharmonic frequency at a temperature approaching 0 K, $\Delta\omega_j(T)_V$ corresponds to the frequency shift from the volume thermal expansion or quasiharmonicity, and $\Delta\omega_j(T)_{anh}$ describes the frequency shift caused by the anharmonic

DOI: 10.1021/acs.jpcc.5b07652
J. Phys. Chem. C 2015, 119, 23094−23102

phonon−phonon coupling, i.e. the explicit anharmonicity or pure temperature effect. The explicit anharmonicity for frequency shift may be simplified by the model proposed by Klemens[33] and extended by Balkanski et al.,[34,35] considering decay of one phonon of frequency ω into two and three phonons in so-called three-phonon and four-phonon processes, respectively, in the expression

$$\Delta\omega_j(T)_{\mathrm{anh}} = A\left(1 + \sum_{l=1}^{2} \frac{1}{e^{\hbar\omega_l/k_BT} - 1}\right) + B\left(1 + \sum_{m=1}^{3} \frac{1}{e^{\hbar\omega_m/k_BT} - 1} + \frac{1}{(e^{\hbar\omega_j/k_BT} - 1)^2}\right) \quad (2)$$

where A and B are the cubic and quartic anharmonic constants specifying the strength of three- and four-phonon decay processes, respectively, the term $1/(e^{\hbar\omega_l/k_BT} - 1)$ in the braces denote the Bose−Einstein phonon population factor, and the ω_l are the frequencies of the phonons involved in the decay channels with energy conservation of $\omega_{oj} = \omega_1 + \omega_2$ and $\omega_{oj} = \omega_1 + \omega_2 + \omega_3$. The frequencies ω_l of the phonons involved in the decay process may be determined via the phonon dispersion curves and phonon density of states with the constraint to conserve both energy and momentum in the decay. The quasiharmonic or thermal expansion contribution to the frequency shift can be written as

$$\Delta\omega_j(T)_V = \omega_{oj}[\exp(-\gamma_{jT}\int_0^T \beta(T')\,dT') - 1] \quad (3)$$

where γ_{jT} is the isotherm mode Gruneisen parameter and β is the volume thermal expansion coefficient. The total anharmonicity of the phonons as a function of temperature at constant pressure can be calculated using the equation[17]

$$\left(\frac{\partial \ln \omega_j}{\partial T}\right)_P = -\beta\gamma_{jT} + \left(\frac{\partial \ln \omega_j}{\partial T}\right)_V \quad (4)$$

The first term of the right-hand side describes the quasiharmonic contribution, and the second term is the explicit anharmonicity.

We estimated the mode Gruneisen parameter γ_{jT} based on the work of Graham et al. They performed pressure-dependent Raman scattering measurements for a PdO film formed on a Pd foil and obtained 1.9 ± 0.1 for the B_{1g} phonon of the material.[36] The parameter was calculated without considering a potential interfacial strain effect on the Raman shift as observed in the present study. By counting a strain effect due to the large difference in the bulk modulus (280 and 180 GPa for PdO and Pd, respectively), we obtained a reduced value of 1.58 for the B_{1g} mode Gruneisen parameter γ_{jT} of PdO by assuming a 50% constrain between the nanoscale thin PdO film and the much thicker Pd foil under isobaric condition (equivalent to an effective 230 GPa bulk modulus for the PdO layer of this sample). The value is consistent with that obtainable from their low-pressure Raman data without counting the interfacial strain effect, as this effect seems low for the sample at this condition. Mode Gruneisen parameters of materials normally change very weakly with temperature and can be considered to be constants for analysis of the quasiharmonic contribution. The thermal expansion coefficient β is unknown for PdO. We thus employed the literature reported lattice constants of PdO, determined by X-ray diffraction in the temperature range from 293 to 1023 K.[37] By fitting the data with a polynomial function, we obtained the lattice constants and volume as a function of temperature in this temperature range. The data were then fitted with the phenomenological analytical expression[38]

$$\beta(T) = \left(\frac{a}{T} + \frac{b}{T^2}\right)\sinh^{-2}\left(\frac{T_1}{T}\right) \quad (5)$$

giving the parameters $a = 7.48 \times 10^{-6}$, $b = 0.041$ K, and $T_1 = 46.8$ K, which fulfills the physical requirement that $\beta \to 0$ at 0 K.

The variation of phonon line width with temperature reveals the information on the phonon relaxation processes.[39] The line width $\Gamma_j(T)$ is given by the negative imaginary part of the anharmonic phonon self-energy and can be similarly reduced to the simple model considering the cubic and quartic phonon decay processes

$$\Gamma_j(T) = \Gamma_{oj} + C\left(1 + \sum_{l=1}^{2} \frac{1}{e^{\hbar\omega_l/k_BT} - 1}\right) + D\left(1 + \sum_{m=1}^{3} \frac{1}{e^{\hbar\omega_m/k_BT} - 1} + \frac{1}{(e^{\hbar\omega_j/k_BT} - 1)^2}\right) \quad (6)$$

where Γ_{oj} is the mode harmonic line width independent of temperature, and the prefactors C and D define the anharmonic constants for line broadening from the three- and four-phonon processes, respectively.

The Klemens model typically assumes a symmetric decay of one optical phonon into acoustic overtones with frequencies $\omega_1 = \omega_2 = \omega_o/2$ and $\omega_1 = \omega_2 = \omega_3 = \omega_o/3$ on the same branch for the cubic and quartic processes,[11,28,35] where the mode index is neglected for simplicity. This is viable for the quartic decay of the B_{1g} mode. However, a lack of the $\omega_o/2$ (~329 cm^{-1}) phonon state in the frequency gap between the optical and acoustic branches of the phonon density of states[10] prohibits such an approximation of overtone states for the cubic decay of this mode. In addition, the overtone density of states is generally low, and symmetric decay channels may have a weak contribution to phonon relaxation processes. Thus, asymmetric decay channels of two-phonon combination including the Ridley decay channel[40−43] should be invoked as a necessity and completion for these decay processes, which allows an insight into the effects of the phonon dispersion on phonon anharmonicity. Both the symmetric decay and the asymmetric phonon decay channels were analyzed with the criteria of energy and momentum conservations through inspection of the phonon dispersion curves and phonon density of states as well as the Raman spectrum reported in ref 10 for PdO. Within these criteria there are potentially multiple asymmetric channels for one phonon to decay. We found that the asymmetric cubic decay channels of the B_{1g} mode are correlated with down-conversion to a pair of optical and acoustic phonons of lower energies with opposite wave vectors, including those along certain directions (e.g., Γ−A, X−M) of the phonon dispersion. Among these channels, B_{1g} (651 cm^{-1}) → AP(X−M) + OP(X−M), where ω(AP) = 140 cm^{-1} and ω(OP) = 511 cm^{-1} is the most contributable because the density of states (DOS) presents maxima at the specified AP and OP frequencies. The asymmetric quartic decay channels of the B_{1g} mode may be identified by assuming that the most likely channels are the decay into a zone-center phonon plus a pair of opposite wave-vector phonons at the zone edges.[40] One such probable quartic decay channel is $B_{1g} \to B_{2u}(\Gamma)$ − TA(X) + TO(X), where

DOI: 10.1021/acs.jpcc.5b07652
J. Phys. Chem. C 2015, 119, 23094−23102

Table 1. Fitting Parameters for the Temperature-Dependent Raman Frequency Shift (Eq 2) and Line Broadening (Eq 6) of the E_g Mode of PdO Crystal, Including the Phonon Properties Extrapolated to 0 K

quartic decay phonon (cm^{-1})		cubic decay phonon (cm^{-1})	A (cm^{-1})	B (cm^{-1})	harmonic ω_o (cm^{-1})	anharmonic ω(0 K) (cm^{-1})	C (cm^{-1})	D (cm^{-1})	Γ_o (cm^{-1})	Γ(0 K) (cm^{-1})
246, −142, 547	M−Γ	114, 537	−1.385	−0.219	657.88	656.14	1.225	0.253	3.99	5.47
			(±0.199)	(±0.032)	(±0.44)	(±0.29)	(±0.06)	(±0.01)	(±0.13)	(±0.03)
		131, 520	−1.557	−0.216	657.96	656.18	1.379	0.251	3.92	5.55
			(±0.21)	(±0.032)	(±0.45)	(±0.29)	(±0.07)	(±0.01)	(±0.13)	(±0.01)
	Γ−A	138, 513	−1.623	−0.215	657.99	656.15	1.44	0.250	3.89	5.58
			(±0.232)	(±0.032)	(±0.45)	(±0.29)	(±0.073)	(±0.01)	(±0.13)	(±0.0)
		173, 478	−1.932	−0.211	658.13	655.98	1.714	0.246	3.77	5.73
			(±0.272)	(±0.032)	(±0.47)	(±0.3)	(±0.091)	(±0.011)	(±0.15)	(±0.04)
	X−M	140, 511	−1.645	−0.215	658	656.13	1.457	0.249	3.88	5.59
			(±0.234)	(±0.032)	(±0.45)	(±0.29)	(±0.074)	(±0.01)	(±0.14)	(±0.01)
	Γ−X	169, 482	−1.907	−0.211	658.12	656	1.691	0.246	3.78	5.71
			(±0.269)	(±0.032)	(±0.47)	(±0.3)	(+0.09)	(+0.011)	(±0.15)	(±0.03)
	R−Z	103, 548	−1.268	−0.215	657.83	656.34	1.122	0.254	4.03	5.41
			(±0.183)	(±0.032)	(±0.44)	(±0.29)	(±0.054)	(±0.01)	(±0.12)	(±0.04)
	X−R	135, 516	−1.597	−0.216	657.93	656.16	1.414	0.250	3.9	5.57
			(±0.228)	(±0.032)	(±0.45)	(±0.29)	(±0.072)	(±0.01)	(±0.13)	(±0.00)
average			−1.614	−0.215	657.98	656.15	1.430	0.250	3.9	5.58
deviation (±)			0.228	0.003	0.10	0.12	0.203	0.003	0.09	0.11
ω_o/3(219)	X−M	140, 511	−1.642	−0.255	658.02	655.71	1.454	0.295	3.86	5.61
			(±0.235)	(±0.036)	(±0.45)	(±0.29)	(±0.074)	(±0.012)	(±0.13)	(±0.0)

$\omega(B_{2u})$ = 246 cm^{-1}, ω(TA) = 142 cm^{-1}, and ω(TO) = 547 cm^{-1}, given by the nearly maximal DOS exhibited at these frequencies. Table 1 lists multiple potential cubic and quartic decay channels for the B_{1g} mode. Note that the list is not complete, and even more decay channels are possible as the dispersion curves only include information related to the directions of high symmetry rather than the entire Brillouin zone.

There may be many combinations from the identified multiple cubic and quartic decay channels for explicit anharmonic study rather than a single or a few combined channels. We chose to combine one asymmetric quartic decay channel with each asymmetric cubic channel to fit the temperature dependence of the Raman spectra, which is compared to the mixed symmetric quartic decay with the asymmetric cubic decay specified above, termed as mixed decay for short. Excellent fittings were obtained for all such combined channels with the fitting parameters and errors summarized in Table 1. This confirms the multiple potential channels and suggests that the cubic and quartic decay channels can work in many combinations contributing to the explicit phonon anharmonicity that fits the experimental data with no constraint on the selection, which is physically reasonable as this should be the nature of fast thermal equilibration through multiple phonon scattering channels. The contribution weight of the different combinations depends on the density of states of the specific phonons that are involved in each combination for the anharmonic process. Figure 7 is the experimental temperature dependencies of the B_{1g} phonon frequency shift and broadening fitted by eqs 1 and 6 with the combination of the cubic and quartic decay channels specified above, B_{1g} (651 cm^{-1}) → AP (140 cm^{-1}) + OP (511 cm^{-1}) and B_{1g} (651 cm^{-1}) → B_{2u} (246 cm^{-1}) − TA (142 cm^{-1}) + TO (547 cm^{-1}). From the fitting results to the experimental data in Figure 7a, it is observed that for the line shift the thermal expansion is the dominant contributor while the cubic anharmonicity contribution is a leading term over the quartic decay. The fit quality (R^2 = 0.9998) indicates that the higher order quartic term in the Hamiltonian is a necessity,[34] as also seen and discussed below from the temperature-dependent line width (Figure 7b). It is noticeable that both the cubic and quartic decays cause the B_{1g} mode to soften or down shift by negative anharmonicities while the quasiharmonicity induces a normal softening of the mode due to a drop of lattice force constant with thermal expansion.[39] For the B_{1g} mode, the cubic decays are found to be down-conversion, i.e., decaying into phonons of lower energy, as

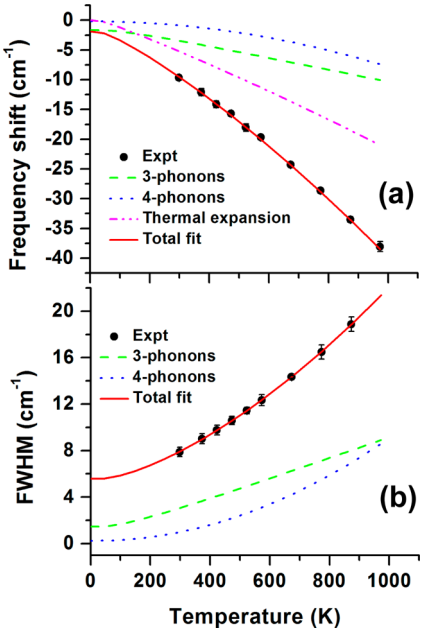

Figure 7. Frequency shift (a) and fwhm (b) of the B_{1g} mode of PdO as a function of temperature. The filled diamonds represent the experimental data, and the solid line is a total theoretical fit including the contributions of three-phonon, four-phonon, and thermal expansion contributions shown as dashed, dotted, and dash/dotted lines, respectively.

DOI: 10.1021/acs.jpcc.5b07652
J. Phys. Chem. C 2015, 119, 23094−23102

noted above, and the quartic decay involves also one down-conversion (Table 1). Although the exact origin is not known, it appears that the negative anharmonicities are associated with down-conversion of phonon decay channels based on the assumption or understanding that with nonequilibrium phonons decaying into those of lower energies the specific interatomic vibration potentials should weaken, perturbing the modes with a downshift from their original line positions or a loss of some energy. If this is true, an up-conversion should cause an upshifting, which is indeed observed from the E_g mode as discussed later.

As shown by Table 1, for all fitted channels, the cubic anharmonic coupling strength A is greater than the quartic strength B, which is expected for bulk materials.[34] In particular, the anharmonic coupling strengths are found to be decay channel specific or characteristic of the channel. This can be seen from the trend that for a fixed quartic decay channel the coupling strength B changes little while the cubic coupling strength A varies with the selection of the cubic channel. The anharmonic coupling strengths along with the Bose−Einstein phonon population factor are required to provide a more complete description of the processes of phonon anharmonic decay into allowed channels to achieve an equilibrium phonon population in materials. Thus, in spite of the variation of the anharmonic coupling strengths with the specific phonon decay channels selected, the contribution of explicit anharmonicity (cubic plus quartic contribution) is typically less than or around 45% for the B_{1g} mode at different temperatures for each asymmetric decay channel combination or the mixed decay, as can be seen from Figure 7a, while the relative cubic and quartic contributions are decreasing and increasing, respectively, with temperature. With the estimated mode Gruneisen parameter, the dominance of the thermal expansion contribution may be evidence that PdO is not described by purely covalent bonding[9,10,44] as quasiharmonicity is generally less prevalent in strongly covalent materials.[45,46] In comparison, for ionically bonded crystals, with nonoverlapping electronic configurations, it is common to have larger thermal expansion contributions over the anharmonicity terms.[47]

The ω_o as obtained through the fitting process changes little with the various decay channel combinations selected for the fitting, giving an average value of 657.9 cm^{-1} for the B_{1g} phonon mode. Though the experimental data were not collected below 300 K, the highly consistent data pinpoint this value likely as the temperature-independent harmonic frequency of the B_{1g} mode of PdO. Noticeably, at 0 K, there is still an anharmonicity that softens the harmonic frequency by −1.83 (±0.23) cm^{-1} given by the combination of the averaged anharmonic constants A and B, although there are no thermally occupied anharmonic phonons at $T \rightarrow 0$. The prediction of a finite phonon line shift at 0 K due to anharmonicity is in agreement with the conclusion derived within the local-density approximation for the iron-pnictide superconductors reported by Granath et al.[48] This indicates that even at zero temperature there are still phonon−phonon scattering processes, producing a finite perturbation to the harmonic phonon frequency or energy.

Table 2 summarizes the result at 298 K on the experimental isobaric frequency shift or total anharmonicity of the B_{1g} mode and the itemized contributions from the quasiharmonicity and the explicit anharmonicity. Consistent with the fitting result exhibited in Figure 7a, the thermal expansion or quasiharmonic contribution is dominant while the explicit anharmonicity is

Table 2. Frequency, Isothermal Mode Gruneisen Parameter, Isobaric Logarithmic Temperature Slope, Pure Volume Contribution, and Explicit Anharmonic Contribution for the B_{1g} Mode of PdO Crystal

mode	ω (cm^{-1})	γ_{jT}[a]	$(\partial \ln(\omega)/\partial T)_P$ (10^{-5} K^{-1})	$-\gamma_{jT}\beta$ (10^{-5} K^{-1})	$(\partial \ln(\omega)/\partial T)_V$ (10^{-5} K^{-1})
B_{1g}	648	1.58	−5.24 ± 0.53	−3.08	−2.16

[a]The mode Gruneisen parameter is estimated from ref 36.

relatively smaller. If an equivalent isobaric Gruneisen parameter γ_{jP} is defined as $-(\partial \ln \omega_j/\partial \ln V)_P = -(1/\beta)(\partial \ln \omega_j/\partial T)_P$,[49] a value of 2.75 ± 0.27 (298 K) can be obtained, which is larger than the isothermal γ_{jT} (1.58) by a factor of 1.74 with their difference resulting from the explicit anharmonicity $(\partial \ln \omega_j/\partial T)_V = \beta(\gamma_{jT} - \gamma_{jP})$ (a different form of eq 4). This factor will be used for estimation of γ_{jT} for the E_g mode as presented later.

Using the same fitting parameter ω_o for the phonon line shift, the parameters Γ_o, C, and D in eq 6 were obtained for each combined phonon decay channel (Table 1). Exhibited in Figure 7b is the experimental B_{1g} phonon line broadening along with the fitting from the representative cubic and quartic phonon decay processes specified above for Figure 7a. As demonstrated, the phonon line broadens quickly at higher temperatures (starting roughly above the Debye temperature, T_D, of 351.79 K for PdO) due to the faster increasing quartic anharmonic phonon−phonon interaction. The data fit illustrates that the higher-order quartic anharmonicity term is indeed an essential component to describe the explicit phonon anharmonicity giving a T^2 dependence of line broadening.[12,50] In Table 1, the cubic anharmonic coupling strengths C for the line broadening is also larger than that of quartic process (D) for each of the combined channels, a feature of bulk crystals as mentioned above. Likewise, for a fixed quartic decay channel, the coupling strength D changes little while the cubic anharmonic coupling strength C varies with the selection of the channel, supporting the finding that an anharmonic phonon decay channel has its own characteristic coupling strength. Combination of the explicit anharmonic coupling strengths and Bose−Einstein phonon population factors describes the experimental line broadening with respective contributions of the cubic and quartic decay processes within a similar Debye temperature regime, as exhibited in Figure 7b, for each specific combination of the decay channels. For the temperature-independent line broadening Γ_o, other than the contribution of the finite resolution of the spectrometer, an average value of 3.9 (±0.09) cm^{-1} was obtained with low deviation within the different combinations of the asymmetric cubic and quartic decay channels listed in Table 1. Again, though there is a lack of the experimental data below 300 K, the highly consistent Γ_o is intrinsic for the B_{1g} mode due to the broadening by the crystalline defects/impurities, which perturb the translation symmetry of the harmonic crystal, making the momentum conservation rule for phonon scattering partially relaxed.[51,52] The presence of the explicit anharmonicity extrapolated at 0 K further broadens the phonon line width to an average of 5.58 (±0.11) cm^{-1} at this extreme temperature.

The Klemens cubic and quartic phonon decays of equal energies holds for the E_g mode as the requisite phonons exist in both the one-phonon and two-phonon density of states of PdO,[10] but we also focused on analyzing the asymmetric decay channels. Unlike that for the B_{1g} mode, the possible asymmetric cubic decay channels are identified to be the type of up-

DOI: 10.1021/acs.jpcc.5b07652
J. Phys. Chem. C 2015, 119, 23094−23102

Table 3. Fitting Parameters for the Temperature-Dependent Raman Frequency Shift (Eq 2) and Line Broadening (Eq 6) of the E_g Mode of PdO Crystal, Including the Phonon Properties Extrapolated to 0 K

quartic decay phonon (cm^{-1})		cubic decay phonon (cm^{-1})	A (cm^{-1})	B (cm^{-1})	harmonic ω_o (cm^{-1})	anharmonic ω(0 K) (cm^{-1})	C (cm^{-1})	D (cm^{-1})	Γ_o (cm^{-1})	Γ(0 K) (cm^{-1})
598, −208, 55	M−Γ		0.459	−0.101	445.37	445.73	1.719	0.096	4.03	5.84
		−153, 598	(±0.419)	(±0.008)	(±0.8)	(±1.13)	(±1.18)	(±0.003)	(±2.12)	(±0.73)
	R		0.358	−0.101	445.42	445.68	1.33	0.097	4.24	5.67
		−118, 565	(±0.32)	(±0.008)	(±0.74)	(±1.23)	(±0.904)	(±0.003)	(±1.95)	(+0.73)
	X−R		0.462	−0.101	445.37	445.73	1.73	0.096	4.02	5.85
		−154, 599	(±0.422)	(±0.008)	(±0.8)	(±1.13)	(±1.19)	(±0.003)	(±2.12)	(±0.73)
			0.4	−0.101	445.4	445.7	1.484	0.096	4.16	5.74
		−132, 577	(±0.36)	(±0.008)	(±0.76)	(±1.19]	(±1.01)	(±0.003)	(±2.01)	(±0.74)
	R−Z		0.309	−0.101	445.44	445.65	1.144	0.097	4.34	5.58
		−101, 546	(±0.276)	(±0.008)	(±0.71)	(±1.28)	(±0.773)	(±0.003)	(±1.87)	(±0.76)
	Γ−A		0.526	−0.101	445.33	445.76	1.983	0.095	3.87	5.95
		−176, 621	(±0.486)	(±0.008)	(±0.84)	(±1.08)	(±1.38)	(±0.003)	(±2.25)	(±0.71)
			0.35	−0.101	445.42	445.67	1.297	0.097	4.26	5.65
		−115, 560	(±0.314)	(±0.008)	(±0.73)	(±1.24)	(±0.881)	(±0.003]	(±1.93)	(±0.75)
	A−Z		0.523	−0.101	445.33	445.76	1.971	0.095	3.88	5.94
		−175, 620	(±0.483)	(±0.008)	(±0.84)	(±1.08)	(±1.37)	(±0.003)	(±2.24)	(±0.71)
average			0.423	−0.101	445.39	445.71	1.582	0.096	4.1	5.78
deviation (±)			0.082	0.000	0.04	0.04	0.316	0.001	0.18	0.14
ω_o/3(147)	ω_o/2	221	0.405	−0.26	445.56	444.18	1.49	0.251	4.24	5.98
			(±0.362)	(±0.003)	(±0.7)	(±1.08)	(±1.02)	(±0.008)	(±1.84)	(±0.69)

conversion, i.e., decaying into a higher energy optical phonon via coupling with a lower energy acoustic phonon. They may include those at the critical point R on the zone edges and along certain directions (e.g., M−Γ, X−R) of the phonon dispersion, for instance, E_g (445 cm^{-1}) → OP (X−R) − AP (X−R), where ω(OP) = 577 cm^{-1} and ω(AP) = 132 cm^{-1}. Using the same assumption for the B_{1g} mode, the possible asymmetric quartic decay channels of the E_g mode involve at least one down-conversion, such as $E_g \rightarrow E_u^2(\Gamma) - X_3(X) + TA(X)$, where $\omega(E_u^2)$ = 598 cm^{-1}, $\omega(X_3)$ = 208 cm^{-1}, and ω_{TO} = 55 cm^{-1}. Though this channel involves a low DOS at 55 cm^{-1}, the Bose−Einstein factor for this channel is high due to the low energy relative to k_BT. The cubic and quartic decay channels for the E_g mode are partially identified and summarized in Table 3.

For the E_g mode, there is no mode Gruneisen parameter γ_{jT} reported so far. We experimentally obtained γ_{jP} of 2.09 (±0.56) for the E_g mode at 298 K and roughly estimated its γ_{jT} to be 1.20 based on the measured data and the ratio of γ_{jP}/γ_{jT} from the B_{1g} mode considering that the two modes display comparably large phonon shifting and broadening (see Figure 6). The obtained result is in agreement with the mode dependence of Gruneisen parameter reported for different materials.[53] Fitting to the experimental data along with extrapolation of the model to 0 K was performed for the temperature dependence of the E_g mode using the estimated mode Gruneisen parameter γ_T for each of the combined cubic and quartic decays channels. This yields the results in Table 3 and representative Figure 8 with fitting quality of R^2 = 0.995, based on the decay of E_g (445 cm^{-1}) → OP (577 cm^{-1}) − AP (132 cm^{-1}) and E_g (445 cm^{-1}) → E_u^2 (598 cm^{-1}) − X_3 (208 cm^{-1}) + TA (55 cm^{-1}). Pure Klemens or symmetric decay leads to very similar results to this but with higher quartic anharmonic coupling parameters characteristic of the higher channel frequency (ω_o/3) as compared to the 55 cm^{-1} for the asymmetric one specified. A noticeable difference for the E_g mode is that the experimental temperature dependence of the

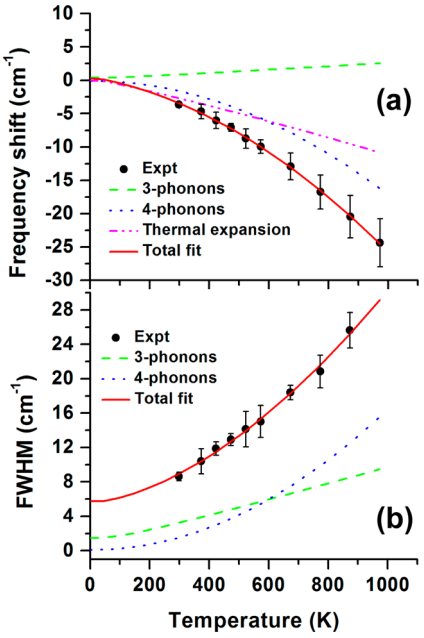

Figure 8. Frequency shift (a) and fwhm (b) of the E_g mode of PdO as a function of temperature. The filled diamonds represent the experimental data, and the solid line is a total theoretical fit including the contributions of three-phonon, four-phonon, and thermal expansion contributions shown as dashed, dotted, and dash/dotted lines, respectively.

line shift is more nonlinear. This trend is found to arise mainly from the quartic phonon decay process as the positive cubic anharmonicity and the negative thermal expansion effect are relatively linearly temperature dependent and partially cancel each other (Figure 8a). Beyond the quasiharmonic contribution, unlike the B_{1g} mode, the E_g mode has an unusual positive explicit anharmonic shift at temperatures below T_D due to the dominance of the cubic decay process having a positive anharmonic phonon coupling strength given by the fitting

DOI: 10.1021/acs.jpcc.5b07652
J. Phys. Chem. C 2015, 119, 23094−23102

parameter *A*. With temperature increasing, the E_g mode changes to the normal negative explicit anharmonic shift, owing to the quickly increasing phonon population factor of the four-phonon coupling process. Adding the quasiharmonicity to the explicit anharmonicity, the phonon is predicted to be hardened at temperature below ~100 K through the modeled extrapolation and is then softened as usual as seen with the experimental data. As reported in the literature, the frequency shift may be either negative or positive depending on the magnitudes and signs of the anharmonic terms in the interatomic potential.[11,54] However, it is still an active aspect to study about the mechanism of unusual positive anharmoniciy in materials, which occurs with the cubic anharmonic phonon−phonon interaction for the E_g mode. By correlating to the detailed decay channels, it appears that the positive cubic anharmonicity arises from the up-conversion of the cubic decays as the phonon-merging conversion produces a higher frequency phonon and may correspondently affect the equilibrating E_g phonon with an upshift from its original frequency in this circumstance, an explanation coherent with that discussed for the B_{1g} mode above. In this process, there are likely a larger number of possible asymmetric up-conversion channels proceeding, which overwhelms the effect of the single symmetric channel that is down-conversion. However, there may have other sources determining the signs of the anhamonic terms.

As shown in Table 3, the fitting of the experimental data with the various combinations of the cubic and quartic decay channels predicts an average of 445.4 cm^{-1} for the temperature-independent harmonic frequency of the E_g mode, a value from which the room temperature anharmonic frequency of this mode downshifts slightly due to the competing anharmonic components and thus smaller net anharmonicity with this mode as opposed to that for the B_{1g} mode. Self-consistent with the fitting for the line shift, the experimental line width of the E_g mode exhibits a larger contribution from the quartic anharmonicity at temperatures above ~T_D (Figure 8b). As a result, the line broadening with temperature is more prominent than that of the B_{1g} mode. The relative contributions of the cubic and quartic decays to the experimental line broadening possess similar T_D regime for the different decay channels combined.

CONCLUSIONS

Raman spectra of tetragonal PdO were measured at temperatures from 298 to 973 K, and the anharmonic behaviors of the B_{1g} and E_g phonon modes were studied. The experimental temperature dependencies of the phonon line shift and broadening of the two modes are represented satisfactorily with a decay model considering quasiharmonic and pure anharmonic terms. Beyond the dominance of the thermal expansion effect, the cubic anharmonicity is found to be leading the quartic anharmonicity for the line shift of the B_{1g} mode. In comparison, the quartic anharmonicity is shown to be the dominant net decay channel for the E_g mode line shift as its positive cubic anharmonicity found is mostly canceled by its negative quasiharmonicity. The temperature-dependent phonon line broadening exhibits an increased contribution from the quartic decay processes. Multiple potential asymmetric cubic decay channels are identified and determined to be down-conversion or up-conversion for the B_{1g} or E_g modes while the quartic decays involve at least one down-conversion for both.

AUTHOR INFORMATION

Corresponding Author

*E-mail: carpenter@sunypoly.edu (M.A.C.).

Notes

The authors declare no competing financial interest.

ACKNOWLEDGMENTS

The authors appreciate Vitor A. Vulcano Rossi for providing the PdO samples. This work was supported by the National Science Foundation Partnerships for Innovation: Building Innovation Capacity (PFI: BIC) subprogram under Grant No. 1318136. Any opinions, findings, and conclusions or recommendations expressed in this material are those of the author(s) and do not necessarily reflect the views of the National Science Foundation.

REFERENCES

(1) Fujimoto, K.-I.; Ribeiro, F. H.; Avalos-Borja, M.; Iglesia, E. Structure and Reactivity of PdO_x/ZrO_2 Catalysts for Methane Oxidation at Low Temperatures. *J. Catal.* **1998**, *179*, 431−442.

(2) Stasinska, B.; Machocki, A.; Antoniak, K.; Rotko, M.; Figueiredo, J. L.; Goncalves, F. Importance of Palladium Dispersion in Pd/Al_2O_3 Catalysts for Complete Oxidation of Humid Low-methane−air Mixtures. *Catal. Today* **2008**, *137*, 329−334.

(3) Osorio, G. P.; Moyado, S. F.; Petranovskii, V.; Simakov, A. $PdO/Al_2O_3-(Ce_{1-X}Zr_X)O_2$ Catalysts: Effect of the Sol-gel Support Composition. *Catal. Lett.* **2006**, *110*, 53−60.

(4) Chin, Y.-H.; Iglesia, E. Elementary Steps, the Role of Chemisorbed Oxygen, and the Effects of Cluster Size in Catalytic CH4!O2 Reactions on Palladium. *J. Phys. Chem. C* **2011**, *115*, 17845−17855.

(5) Kinnunen, N. M.; Hirvi, J. T.; Suvanto, M.; Pakkanen, T. A. Role of the Interface between Pd and PdO in Methane Dissociation. *J. Phys. Chem. C* **2011**, *115*, 19197−19202.

(6) Kurzman, J. A.; Misch, L. M.; Seshadri, R. Chemistry of Precious Metal Oxides Relevant to Heterogeneous Catalysis. *Dalton Trans.* **2013**, *42*, 14653−14667.

(7) Spirig, J. V.; Ramamoorthy, R.; Akbar, S. A.; Routbort, J. L.; Singh, D.; Dutta, P. K. High Temperature Zirconia Oxygen Sensor with Sealed Metal/Metal Oxide Internal Reference. *Sens. Actuators, B* **2007**, *124*, 192−201.

(8) Moore, W. J.; Pauling, L. The Crystal Structures of the Tetragonal Monoxides of Lead, Tin, Palladium, and Platinum. *J. Am. Chem. Soc.* **1941**, *63*, 1392−1394.

(9) Kurzman, J. A.; Miao, M. S.; Seshadri, R. Hybrid Functional Electronic Structure of $PbPdO_2$, a Small-gap Semiconductor. *J. Phys.: Condens. Matter* **2011**, *23*, 465501.

(10) McBride, J. R.; Hass, K. C.; Weber, W. H. Resonance-Raman and Lattice-dynamics Studies of Single-crystal PdO. *Phys. Rev. B: Condens. Matter Mater. Phys.* **1991**, *44*, 5016−5029.

(11) Maczka, M.; Ptak, M.; Pereira da Silva, K. ; Freire, P. T. C.; Hanuza, J. High-pressure Raman Scattering and an Anharmonicity Study of Multiferroic Wolframite-type $Mn_{0.97}Fe_{0.03}WO_4$. *J. Phys.: Condens. Matter* **2012**, *24*, 345403.

(12) Tang, H.; Herman, I. P. Raman Microprobe Scattering of Solid Silicon and Germanium at the Melting Temperature. *Phys. Rev. B: Condens. Matter Mater. Phys.* **1991**, *43*, 2299−2304.

(13) Bertheville, B.; Bill, H.; Hagemann, H. Experimental Raman Scattering Investigation of Phonon Anharmonicity Effects in Li_2S. *J. Phys.: Condens. Matter* **1998**, *10*, 2155−2169.

(14) Chen, Y.; Peng, B.; Wang, B. Raman Spectra and Temperature-Dependent Raman Scattering of Silicon Nanowires. *J. Phys. Chem. C* **2007**, *111*, 5855−5858.

(15) Link, A.; Bitzer, K.; Limmer, W.; Sauer, R.; Kirchner, C.; Schwegler, V.; Kamp, M.; Ebling, D. G.; Benz, K. W. Temperature Dependence of the E_2 and A_1 (LO) Phonons in GaN and AlN. *J. Appl. Phys.* **1999**, *86*, 6256−260.

DOI: 10.1021/acs.jpcc.5b07652
J. Phys. Chem. C 2015, 119, 23094−23102

(16) Lin, J.; Guo, L.; Huang, Q.; Jia, Y.; Li, K.; Lai, X.; Chen, X. Anharmonic Phonon Effects in Raman Spectra of Unsupported Vertical Graphene Sheets. *Phys. Rev. B: Condens. Matter Mater. Phys.* **2011**, *83*, 125430.
(17) Peercy, P. S.; Morosin, B. Pressure and Temperature Dependences of the Raman-Active Phonons in SnO_2. *Phys. Rev. B* **1973**, *7*, 2779−2786.
(18) Sahoo, S.; Gaur, A. P. S.; Ahmadi, M.; Guinel, M. J.-F.; Katiyar, R. S. Temperature-Dependent Raman Studies and Thermal Conductivity of Few-Layer MoS_2. *J. Phys. Chem. C* **2013**, *117*, 9042−9047.
(19) Pintschovius, L. Electron−phonon Coupling Effects Explored by Inelastic Neutron Scattering. *Phys. Status Solidi B* **2005**, *242*, 30−50.
(20) Wang, R. P.; Xu, G.; Jin, P. Size Dependence of Electron-phonon Coupling in ZnO Nanowires. *Phys. Rev. B: Condens. Matter Mater. Phys.* **2004**, *69*, 113303−113306.
(21) Lazzeri, M.; Piscanec, S.; Mauri, F.; Ferrari, A. C.; Robertson, J. Phonon Linewidths and Electron-phonon Coupling in Graphite and Nanotubes. *Phys. Rev. B: Condens. Matter Mater. Phys.* **2006**, *73*, 155426−155431.
(22) Domenech-Amador, N.; Cusco, R.; Artus, L.; Yamaguchi, T.; Nanishi, Y. Raman Scattering Study of Anharmonic Phonon Decay in InN. *Phys. Rev. B: Condens. Matter Mater. Phys.* **2011**, *83*, 245203.
(23) Reihani, S. A. S.; Jackson, G. S. Low-temperature Combustion of Hydrogen on Supported Pd Catalysts. *Proc. Combust. Inst.* **2002**, *29*, 989−996.
(24) Ciuparu, D.; Pfefferle, L. Temperature and Time Dependence of the Water Inhibition Effect on Supported Palladium Catalyst for Methane Combustion. *Appl. Catal., A* **2001**, *216*, 209−215.
(25) Farrauto, R. J.; Hobson, M. C.; Kennelly, T.; Waterman, E. M. Catalytic Chemistry of Supported Palladium for Combustion of Methane. *Appl. Catal., A* **1992**, *81*, 227−237.
(26) Bardhan, R.; Zarick, H. F.; Schwartzberg, A.; Pint, C. L. Size-Dependent Phononic Properties of PdO Nanocrystals Probed by Nanoscale Optical Thermometry. *J. Phys. Chem. C* **2013**, *117*, 21558−21568.
(27) Su, L.; Zhang, Y.; Yu, Y.; Cao, L. Dependence of Coupling of Quasi 2-D MoS_2 with Substrates on Substrate Types, Probed by Temperature Dependent Raman Scattering. *Nanoscale* **2014**, *6*, 4920−4927.
(28) Nikolenko, A. S. Temperature Dependence of Raman Spectra of Silicon Nanocrystals in Oxide Matrix. *Ukr. J. Phys.* **2013**, *58*, 980−986.
(29) Remillard, J. T.; Weber, W. H.; McBride, J. R.; Soltis, R. E. Optical Studies of PdO Thin Films. *J. Appl. Phys.* **1992**, *71*, 4515.
(30) Maradudin, A. A.; Fein, A. E. Scattering of Neutrons by an Anharmonic Crystal. *Phys. Rev.* **1962**, *128*, 2589−608.
(31) Cowley, R. A. Anharmonicity. *J. Phys. (Paris)* **1965**, *26*, 659−664.
(32) Menendez, J.; Cardona, M. Temperature Dependence of the First-order Raman Scattering by Phonons in Si, Ge, and α−Sn: Anharmonic Effects. *Phys. Rev. B: Condens. Matter Mater. Phys.* **1984**, *29*, 2051−2059.
(33) Klemens, P. G. Anharmonic Decay of Optical Phonons. *Phys. Rev.* **1966**, *148*, 845−848.
(34) Balkanski, M.; Wallis, R. F.; Haro, E. Anharmonic Effects in Light Scattering Due to Optical Phonons in Silicon. *Phys. Rev. B: Condens. Matter Mater. Phys.* **1983**, *28*, 1928−1934.
(35) Zouboulis, E. S.; Grimsditch, M. Raman Scattering in Diamond up to 1900 K. *Phys. Rev. B: Condens. Matter Mater. Phys.* **1991**, *43*, 12490−12493.
(36) Graham, G. W.; O'Neill, A. E.; Uy, D.; Weber, W. H.; Sun, H.; Pan, X. Q. Observation of Strained PdO in an Edged PdO/Ceria−zirconia Catalyst. *Catal. Lett.* **2002**, *79*, 99−105.
(37) Rogers, D. B.; Shannon, R. D.; Gillson, J. L. Crystal Growth and Semiconductivity of Palladium Oxide. *J. Solid State Chem.* **1971**, *3*, 314−316.
(38) Liarokapis, E.; Anastassakis, E.; Kourouklis, G. A. Raman Study of Phonon Anharmonicity in LaF_3. *Phys. Rev. B: Condens. Matter Mater. Phys.* **1985**, *32*, 8346−8355.
(39) Lucazeau, G. Effect of Pressure and Temperature on Raman Spectra of Solids: Anharmonicity. *J. Raman Spectrosc.* **2003**, *34*, 478−496.
(40) Domenech-Amador, D.; Cusco, R.; Artus, L.; Yamaguchi, T.; Nanishi, Y. Raman Scattering Study of Anharmonic Phonon Decay in InN. *Phys. Rev. B: Condens. Matter Mater. Phys.* **2011**, *83*, 245203.
(41) Ridley, B. K. The LO Phonon Lifetime in GaN. *J. Phys.: Condens. Matter* **1996**, *8*, L511.
(42) Barman, S.; Srivastava, G. P. Long-wavelength Nonequilibrium Optical Phonon Dynamics in Cubic and Hexagonal Semiconductors. *Phys. Rev. B: Condens. Matter Mater. Phys.* **2004**, *69*, 235208.
(43) Jiménez, J.; Wang, B.; Callahan, M. J. Temperature Dependence of Raman Scattering in ZnO. *Phys. Rev. B: Condens. Matter Mater. Phys.* **2007**, *75*, 165202.
(44) Bauschlicher, C. W., Jr.; Nelin, C. J.; Bagus, P. S. Transition Metal Oxides: CrO, MoO, NiO, PdO, AgO. *J. Chem. Phys.* **1985**, *82*, 3265−3276.
(45) Ramond, T. M.; Davico, G. E.; Hellberg, F.; Svedberg, F.; Salén, P.; Söderqvist, P.; Lineberger, W. C. Photoelectron Spectroscopy of Nickel, Palladium, and Platinum Oxide Anions. *J. Mol. Spectrosc.* **2002**, *216*, 1−14.
(46) Raptis, Y. S.; Kourouklis, G. S.; Anastassakis, E.; Haro-Poniatowski, E.; Balkanski, M. Anharmonic Effects in Mg_2X (X = Si, Ge, Sn) Compounds Studied by Raman Spectroscopy. *J. Phys. (Paris)* **1987**, *48*, 239−245.
(47) Kourouklis, G. A.; Anastassakis, E. Pressure-induced Phase Transition in SrF_2: A Raman Study. *Phys. Rev. B: Condens. Matter Mater. Phys.* **1986**, *34*, 1233−1237.
(48) Granath, M.; Bielecki, J.; Holmlund, J.; Börjesson, L. Anharmonic Softening of Raman Active Phonons in Iron-Pnictides: Estimating the Fe Isotope Effect due to Anharmonic Expansion. *Phys. Rev. B: Condens. Matter Mater. Phys.* **2009**, *79*, 235103.
(49) Gillet, P.; Guyot, F.; Wang, Y. Microscopic Anharmonicity and Equation of State of $MgSiO_3$-perovskite. *Geophys. Res. Lett.* **1996**, *23*, 3043−3046.
(50) Ipatova, I. P.; Maradudin, A. A.; Wallis, R. F. Temperature Dependence of the Width of the Fundamental Lattice-Vibration Absorption Peak in Ionic Crystals. II. Approximate Numerical Results. *Phys. Rev.* **1967**, *155*, 882−895.
(51) Millot, M.; Tena-Zaera, R.; Munoz-Sanjose, V. ; Broto, J.-M.; Gonzalez, J. Anharmonic Effects in ZnO Optical Phonons Probed by Raman Spectroscopy. *Appl. Phys. Lett.* **2010**, *96*, 152103.
(52) Samanta, K.; Bhattacharya, B.; Katiyar, R. S. Temperature Dependent E2 Raman Modes in the ZnCoO Ternary Alloy. *Phys. Rev. B: Condens. Matter Mater. Phys.* **2007**, *75*, 035208.
(53) Kojitani, H.; Többens, D. M.; Akaogi, M. High-pressure Raman Spectroscopy, Vibrational Mode Calculation, and Heat Capacity Calculation of Calcium Ferrite-type $MgAl_2O_4$ and $CaAl_2O_4$. *Am. Mineral.* **2013**, *98*, 197−206.
(54) Yuksek, N. S.; Gasanly, N. M.; Ozkan, H. Temperature Dependence of Raman-active Modes of $TlGaS_2$ Layered Crystals: an Anharmonicity Study. *J. Korean Phys. Soc.* **2004**, *45*, 501−506.

DOI: 10.1021/acs.jpcc.5b07652
J. Phys. Chem. C 2015, 119, 23094−23102